Inerter-based Configurations for Main Landing Gear Shimmy Suppression

Yuan Li*, Jason Zheng Jiang† and Simon Neild‡
University of Bristol, Bristol, BS8 1TR, United Kingdom

The work reported in this paper concentrates on the possibility of suppressing landing gear shimmy oscillations more effectively using a linear passive suppression device incorporating inerter. The inerter is a one-port mechanical device with the property that the applied force is proportional to the relative acceleration between its terminals. A linear model of a Fokker 100 aircraft main landing gear equipped with a shimmy suppression device is presented. Time-domain optimizations of the shimmy suppression device are carried out using cost functions of the maximum amplitude and the settling time of torsional-yaw motion. Applying two types of excitations which trigger the shimmy oscillations, performance advantages of inerter-based configurations for suppressing main landing gear shimmy, together with corresponding parameter values, are identified.

I. Introduction

When an aircraft is operating on the ground, the landing gear may experience a kind of self-induced oscillatory motion, which is well known as shimmy. Under certain operation conditions, such phenomenon can result in instability of the system and impact various components, reducing the fatigue life or in some extreme cases, leading to severe structural failure [1]. In most shimmy analysis work, the landing gear designers and researchers were more interested in forecasting the

* Ph.D. Student, Department of Mechanical Engineering, yl14470@birstol.ac.uk.
† Lecturer of Dynamics and Control, Department of Mechanical Engineering, z.jiang@birstol.ac.uk.
‡ Professor of Dynamics and Control, Department of Mechanical Engineering, simon.neild@birstol.ac.uk.

occurrence of shimmy instability and investigating how to avoid it. However, even when the system does not encounter an instability, severe transient response can still cause component degradation or passenger discomfort. The main interest of this work is to investigate the vibration suppression of these transient oscillations.

The earliest work on shimmy phenomenon was conducted on automotive industry by Broulhiet [2] who included the tire dynamics in shimmy analysis. This is still used in the shimmy analysis of a wide range of wheeled vehicles now and much efforts have been made to model tire-ground contact dynamics accurately (examples can be found in [3–6]). In the 1930s, aircraft nose landing gear shimmy triggered significant research work with the development of tricycle landing gear. Fromm [7] presented the similarities between shimmy in cars and aircraft and led the shimmy analysis into the aerospace field. Even though shimmy oscillations are more oftenly observed on nose landing gears [8], the main landing gears of some types of aircraft, such as Douglas DC-9, Fokker 28, BAC 1-11 and Boeing 737, still suffered from shimmy oscillations [9]. Examples of shimmy events in main landing gears can also be found in [10, 11].

Various control methods have been used for solving the shimmy instability problem, such as the shimmy damper [12–15]. Specifically, the damping effect seems to be of particular significance in the shimmy damper design [14, 15]. More recently, some simple control methods, such as PD control [16] and adaptive control [17], have been used to control shimmy oscillations. It is worth to keep in mind that such control methods may require increased maintenance costs and result in less reliability. Apart from the controllers, the influence of the gear structural characteristics [8, 15] also plays an important role in stabilizing the shimmy-prone gears.

In this work, we propose the use of the inerter in shimmy suppression devices and consider the potential benefits of the inclusion. The inerter is defined as a one-port mechanical element with the property that the applied force is proportional to the relative acceleration between its two terminals, i.e. $F = b(\dot{v}_2 - \dot{v}_1)$ [18]. With the introduction of the inerter, a complete analogy between mechanical system and electrical system can be achieved. Thus, a much wider range of passive absorber structures can be realized by mechanical networks. Beneficial configurations have been identified for various mechanical and civil systems, including vehicle suspensions [19–21],

motorcycle steering systems [22, 23] and building suspensions [24, 25]. A parallel inerter-spring-damper suspension system has been successfully deployed in Formula One racing since 2005 [26]. Such a parallel layout is also proposed as one of the candidate shimmy suppression device layouts in this paper.

This paper is organized as follows. A model of the Fokker 100 main landing gear (MLG) is presented in Section II. In addition, three candidate shimmy suppression layouts are introduced. In Section III, eigenvalue optimization has been carried out to illustrate the limitation of frequency-domain analysis for this problem. Two time-domain performance measures representing the MLG shimmy motion are proposed in Section IV. Beneficial shimmy suppression configurations are identified based on optimization results. Conclusions have been drawn in Section V.

II. A main landing gear model and candidate shimmy suppression layouts

In this section, a model of the Fokker 100 MLG equipped with a shimmy suppression device was presented based on the work by Van der Valk and Pacejka [11]. Three candidate layouts of shimmy suppression devices are also introduced.

A. Description of the dynamic system

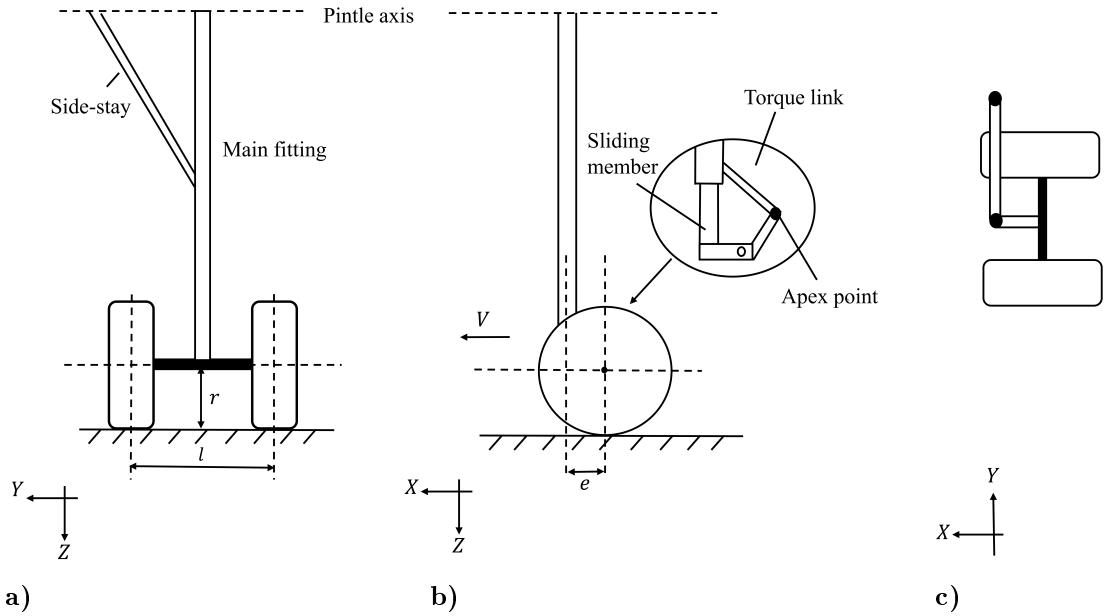

Fig. 1 Schematic view of the dual-wheel Fokker 100 MLG geometry.

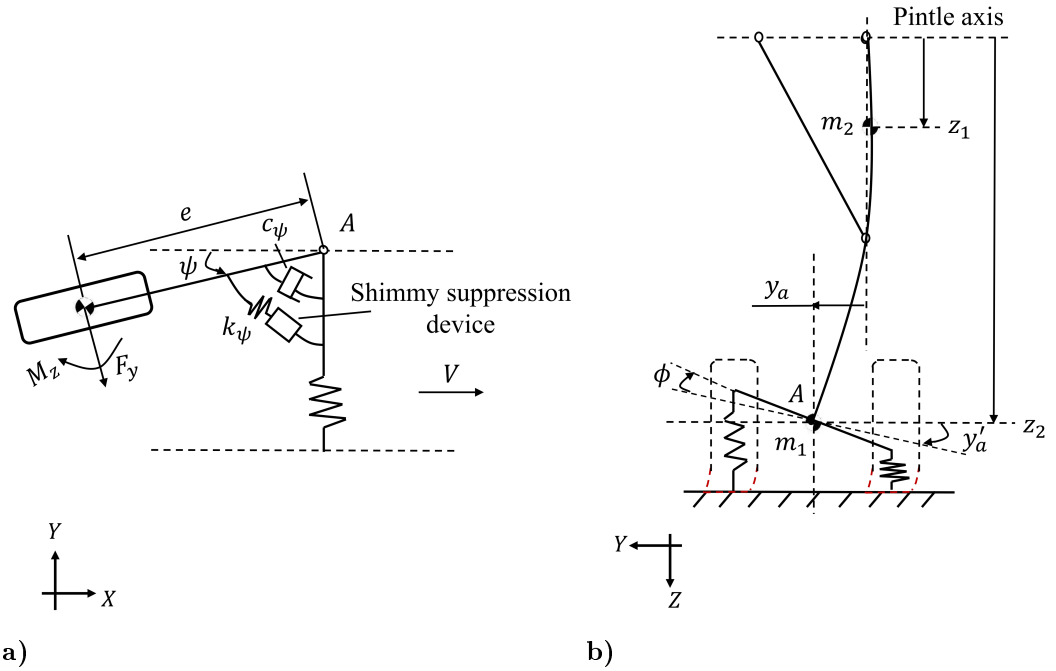

Fig. 2 a) Torsional-yaw ψ DOF, b) lateral deflection of A y_a and roll ϕ DOF (a modified version of Figs. 2 and 3 in [11]).

The geometry of the Fokker 100 MLG is illustrated in Fig. 1 through different views. The structure consists of a main fitting, side-stay, sliding member, axle assembly, etc. The side-stay laterally supports the main fitting and is fixed on the pintle. The sliding member allows both translational and rotational motions with respect to the main fitting. The two wheels are connected by the wheel axle which is offset from the main fitting axis via a mechanical trail bar of length e. The shimmy suppression device, conventionally a shimmy damper, is installed at the torque link apex point (as shown in Fig. 1b). A global coordinate frame (XYZ) is considered and its origin is fixed to the pintle axle. The X axis points in the direction of aircraft forward direction, the Z axis vertically downwards, and the Y axis completes the right-handed coordinate system. The wheel axle of the MLG is allowed to rotate torsionally about the centre line of the main fitting by the angle ψ (torsional-yaw DOF) and to deflect laterally by the displacement y. Modal coordinate η is used to indicate the MLG lateral DOF and will be discussed later. In addition, the wheel axle is allowed to rotate about an axis fixed along the trail bar by the angle ϕ (torsional-roll DOF). These three DOFs represent the MLG motions and are coupled via the tire lateral deformation. Figure 2 illustrates the sign conventions of these DOFs and the tire lateral deformation. In Fig. 2a the two wheels are

collapsed into one plane with respect to the point A. Note that in this model, the fuselage dynamics are ignored and a tire-ground contact constraint is assumed. The interaction between the landing gear shimmy modes and the fuselage dynamics is considered in [27]. Moreover, no axial compression of the strut is considered in the model.

In this model, $c_{\psi,\phi}$, $k_{\psi,\phi}$ are introduced to represent the damping and stiffness of the ψ and ϕ DOFs. Note that in this study we use the conventional notification k for spring and c for damper, different from the ones used in [11] (c for spring and k for damper). Due to the offset between the strut axis and the wheel axle, along with the coupling effects of rolling wheels, the total torsional-yaw moment of inertia is

$$I_{\psi tot} = I_{\psi} + m_1 e^2 + \frac{1}{2} I_{yb} (\frac{l}{r})^2, \tag{1}$$

where the lengths of l and r are defined in Fig. 1, I_{ψ} is the moment of inertia of the wheels, axle and brake assembly, m_1 the unsprung mass and I_{yb} polar moment of inertia of the wheels, axle and brake. As for the MLG lateral motion, the gear lateral bending deflection is expressed by

$$y(z,t) = f(z)\eta(t), \tag{2}$$

where $f(z)$ denotes the approximate mode shape belonging to the first mode of the freely hanging landing gear. The landing gear is regarded as a beam with two concentrated masses: unsprung mass m_1 and the main fitting m_2 (see Fig. 2b) with their mode shapes, $f(z_1)$ and $f(z_2)$, respectively. Thus from Rayleigh's method, the energy terms representing the lateral mode can be expressed in terms of the corresponding modal mass m_f, which can be written as

$$m_f = m_1 f^2(z_1) + m_2 f^2(z_2). \tag{3}$$

The lateral deflection and slope at the shock strut bottom point A, y_a and $y_a{}'$, are specified by the following equations:

$$y_a = f(z_1)\eta, \tag{4}$$

$$y_a{}' = f'(z_1)\eta, \tag{5}$$

where $f'(z_1)$ is the modal slope of A. For the purpose of comparison, it is convenient to consider y_a to represent the MLG physical lateral deflection, instead of η DOF. Moreover, as shown in Fig. 2b,

both ϕ and $y_a{}'$ contribute to the overall roll deflection angle of A, ϕ', giving

$$\phi' = \phi + f'(z_1)\eta. \tag{6}$$

To illustrate the physical effects of this angle, the roll stroke δ at the ground level is considered, as given by

$$\delta = r\,tan\phi'. \tag{7}$$

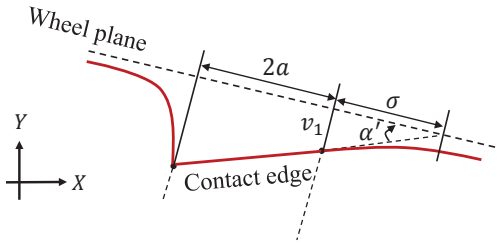

Fig. 3 Schematic of the straight tangent tire model.

The wheel rolling effects are considered in this model. With the assumption of zero tire longitudinal slip, the angular velocity of the wheel Ω is given by the expression

$$\Omega = \frac{V}{R_e}, \tag{8}$$

where R_e is the effective radius of the tire and V is the aircraft forward speed. For the expression of R_e, the empirical equation

$$R_e = R - \frac{1}{3}d \tag{9}$$

can be used, where R is the tire unloaded radius, $d = R - r$ is the tire deflection, see Currey [28]. In this study, the straight tangent tire model is used to describe the tire-ground contact dynamics. The reaction forces produced by the tires can be modelled by the tire lateral deformation. These forces are the lateral force F_y and the tire self-aligning moment M_z, as shown in Fig. 2a, and may be expressed as

$$F_y = C_{F\alpha}\alpha', \tag{10}$$

$$M_z = -C_{M\alpha}\alpha', \tag{11}$$

where $\alpha^{'}$ is the lateral deflection angle of the leading point of tire-ground contact edge, as shown in Fig. 3. The lateral displacement of the leading point of contact edge, v_1, is considered to represent the tire lateral deformation when investigating the physical shimmy motion. It can be expressed as

$$v_1 = \alpha^{'}\sigma, \tag{12}$$

where σ is the tire relaxation length, as illustrated in Fig. 3. Note that if the MLG is in its undisturbed state, the tire slip angle α is equal to $\alpha^{'}$.

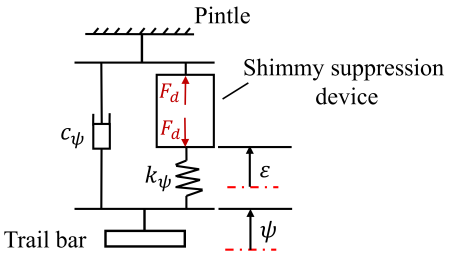

Fig. 4 View of ψ, ε DOFs and k_ψ, where at equilibrium, $\varepsilon = \psi = 0$ and $F_d = 0$ (inspired by [11]).

Table 1 Some system parameter values used in the analysis

Parameter	Name	Value
c_ψ	Torsional-yaw damping value for the gear	1.06×10^3 N·m·s/rad
c_ϕ	Torsional-roll damping value for the gear	5.4×10^2 N·m·s/rad
k_v	Tire vertical stiffness	8.64×10^5 N·m/rad
k_ψ	Overall torsional-yaw structural stiffness for the gear	6.45×10^5 N·m/rad
k_ϕ	Torsional-roll structural stiffness for the gear	2.15×10^6 N·m/rad
f_η	First natural frequency of hanging landing gear	72.0 Hz
ζ_n	First relative damping coefficient for the lateral mode	0.05

The shimmy suppression device is fitted in the apex location which is between the upper and lower torque link. To capture both the structural stiffness of these two parts, an effective torsional-yaw stiffness k_ψ is considered connecting the shimmy suppression device and the unsprung mass as shown in Fig. 2a. The compression of the shimmy suppression device is represented by the torsional DOF ε, see Fig. 4. The force generated by the shimmy suppression device is denoted as F_d. It is the

dynamics of the device, which are captured by the relationship between F_d and ε, and their effects on shimmy oscillations are of primary interest here.

B. Equations of motion

Similar to [11], using Lagrange's method, the corresponding equations of motion for the MLG can be written as

$$I_{\psi tot}\ddot{\psi} - m_1 e f(z_1)\ddot{\eta} + c_\psi\dot{\psi} + 2I_{yb}\Omega(f^{'}(z_1)\dot{\eta} + \dot{\phi}) + k_\psi(\psi - \varepsilon) - 2(eC_{F\alpha} + C_{M\alpha})\alpha^{'} = 0, \tag{13}$$

$$(m_f + I_\phi f^{'2}(z_1))\ddot{\eta} - m_1 e f(z_1)\ddot{\psi} + I_\phi f^{'}(z_1)\ddot{\phi} - 2I_{yb}\Omega f^{'}(z_1)\dot{\psi} + 2m_f\zeta_n f_\eta\dot{\eta}$$
$$+ {f_\eta}^2 m_f\eta + 2C_{F\alpha}(f(z_1) + r f^{'}(z_1))\alpha^{'} + \frac{1}{2}k_v l^2 f^{'}(z_1)(f^{'}(z_1)\eta + \phi) = 0, \tag{14}$$

$$I_\phi(\ddot{\phi} + f^{'}(z_1)\ddot{\eta}) - 2I_{yb}\Omega\dot{\psi} + c_\phi\dot{\phi} + \frac{1}{2}k_v l^2(f^{'}(z_1)\eta + \phi) + k_\phi\phi + 2rC_{F\alpha}\alpha^{'} = 0, \tag{15}$$

$$\sigma\dot{\alpha}^{'} + V(\psi + \alpha^{'}) - (f(z_1) + r f^{'}(z_1))\dot{\eta} - r\dot{\phi} + (e - a)\dot{\psi} = 0, \tag{16}$$

$$F_d - k_\psi(\psi - \varepsilon) = 0. \tag{17}$$

Here, Eqs. (13-15) govern the MLG dynamics and (16) the tire dynamics. Eq. (17) represents the fact that the force across k_ψ equals the force across the shimmy suppression device. The mathematical expression for F_d depends on the layout of shimmy suppression device and will be presented in Section II.C.

In summary, there are 5 DOFs in the equations of motion, which are ψ for the MLG torsional-yaw motion, η for the gear lateral motion, ϕ for the torsional-roll motion, $\alpha^{'}$ for the tire dynamics and ε for the shimmy suppression device motion. The states we actually consider as physical shimmy motions are ψ, y_a, δ and v_1, which are the torsional-yaw deflection, the lateral bending deflection of the point A, the roll stroke of A on the ground and the tire lateral deformation, respectively. The parameter values used in this study are consistent with [11] (with a 0.25 m shock absorber deflection). Several parameters that are not specified in [11] are summarized in Table 1. Note that the aircraft operation condition considered in this study is $V = 50\,\mathrm{m/s}$.

C. Optimization procedure and candidate shimmy suppression layouts

The introduction of an inerter alongside the conventional spring and damper guarantees that any positive-real frequency transfer function can be realized by a network layout consisting of springs, dampers and inerters [29]. The force-displacement relationship of the candidate shimmy suppression devices can be represented by general positive-real functions, $Y(s)$, satisfying

$$\overline{F_d}(s) = Y(s)\bar{\varepsilon}(s), \tag{18}$$

where s is the Laplace variable and $\overline{F_d}(s)$ and $\bar{\varepsilon}(s)$ represent the force and the relative displacement of the device in Laplace domain respectively. For example, the transfer function of the default shimmy damper in the Laplace domain may be written as

$$Y(s) = \frac{\overline{F_d}(s)}{\bar{\varepsilon}(s)} = k + cs. \tag{19}$$

The approach we use to select $Y(s)$ is to select a general transfer function form and then optimize its parameters. Network synthesis theory [30, 31] can then be used to identify the specific layout which can realize the optimized $Y(s)$. For all the optimizations carried out in the present work, we used the Matlab command patternsearch first and then fminsearch for fine-tuning of the parameters. As patternsearch tends to find local minima, the best solutions have been verified using a range of initial starting points.

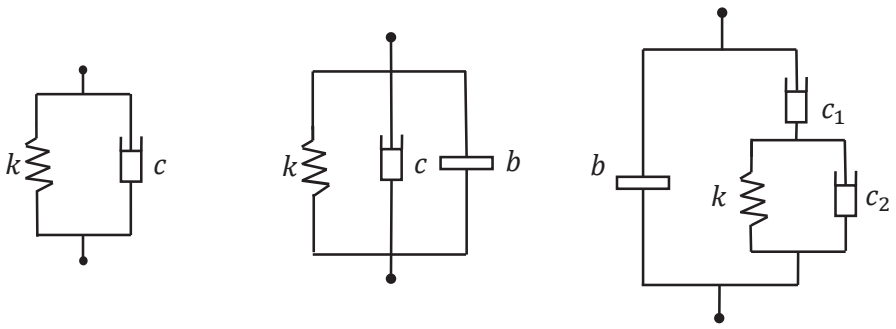

Fig. 5 Three low-complexity layouts of the shimmy suppression device

Since low-complexity networks are more preferable due to the weight and space limit of the landing gear system, a biquadratic function (where both the numerator and denominator are second

order functions of the Laplace operator)

$$Y(s) = \frac{As^2 + Bs + C}{Ds^2 + Es + F} \tag{20}$$

is considered. Applying relevant network synthesis techniques, such as results presented in [32, 33], beneficial layouts can be identified. In this way, we guarantee that a wide range of low-complexity layouts is considered. For most cases, the optimum parameter values (A, B, $\cdots$, F) do not equal zero. The corresponding network normally contains at least five elements. A simplification procedure is then used, to check whether reducing the number of elements results in significant deterioration of performance. A similar procedure can be found in, for example, [34]. A simpler hence more realistic structure can possibly be obtained through this process. A second round optimization of the element values is then performed for the simplified network layout. According to the optimization results, it is interesting to see that layout S2 shown in Fig. 5 is capable of providing promising performance advantages. Even though other more complicated layouts can provide slightly better performances, we take the view that this does not justify the extra complexity of the device. Layout S1 in Fig. 5 represents the conventional shimmy damper layout. Layout S3 is the layout obtained through the eigenvalue optimization of Eq. (20), which will be discussed in Section III. It will be shown that while this layout can significantly increase the least damping ratio, the overall physical response is not significantly improved. Consequently, discussions will focus on layout S2 in Section IV.

III. Limitation of eigenvalue optimization

As the dynamic model is linear, eigenvalue analysis can be carried out. The equations of motion shown in Eqs. (13-17) can be expressed in the following state-space form,

$$\dot{X} = TX, \tag{21}$$

where $X = \left(\dot{\psi}\ \dot{\eta}\ \dot{\phi}\ \psi\ \eta\ \phi\ \alpha'\ \varepsilon\right)^T$ and T is a 8×8 matrix. Applying the Laplace transformation to Eq. (21), the system characteristic equation can be written in terms of the Laplace variable.

It can be checked that using the default shimmy damper parameters taken from [11], with $V = 50\,\mathrm{m/s}$, the least damping ratio ζ_{min} amongst all the modes equals 4.4%. Optimization is carried out to maximize the least damping ratio ζ_{min} with Eq. (20) representing the shimmy

suppression device. The optimization results are given in Table 2. Layout S3 in Fig. 5, with parameter values in row 2 of Table 2, is obtained via network synthesis to realize the specific biquadratic function identified by optimization. It can be seen that that a 77.3% improvement on ζ_{min} can be achieved.

Table 2 Optimization results for maximising ζ_{min}

Layouts	ζ_{min}, %	Improvement, %	Parameter values, N·m/rad, N·m·s/rad, N·m·s^2/rad
Default	4.4	-	$k = 1.9 \times 10^5, c = 7.4 \times 10^3$
S3	7.8	77.3	$k = 1.5 \times 10^5, c_1 = 4.9 \times 10^3, c_2 = 1.0 \times 10^3$
			$b = 13.3$

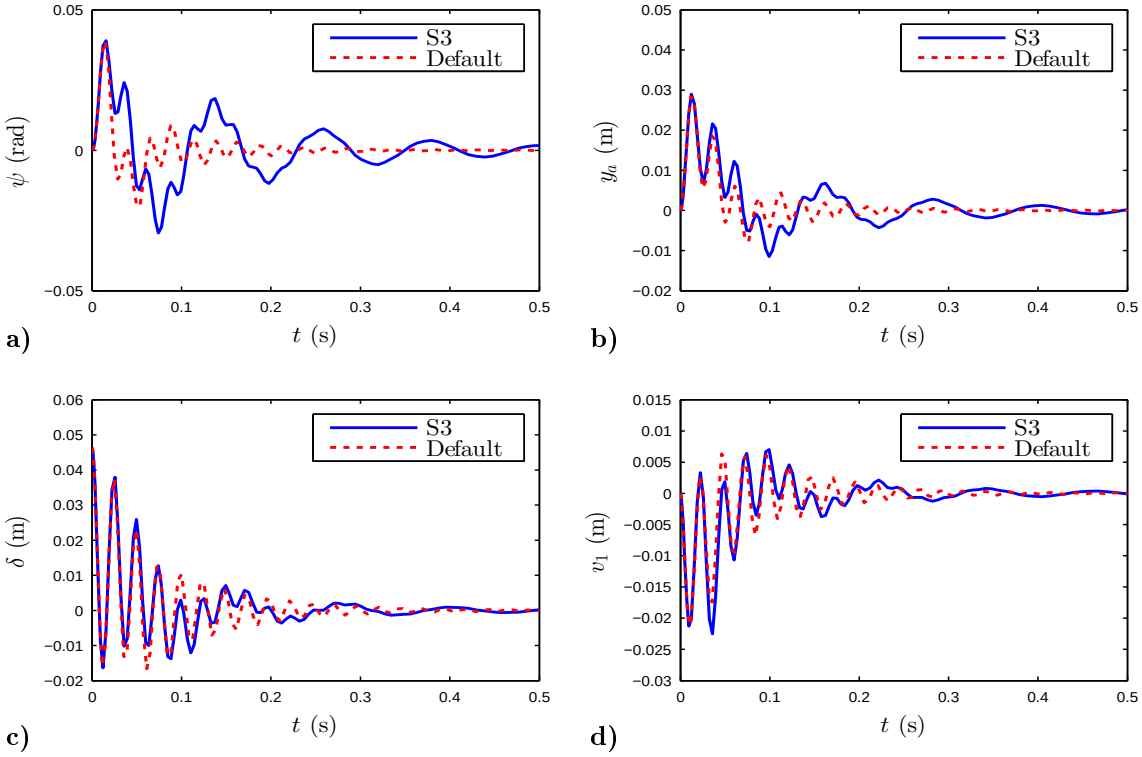

Fig. 6 Comparison of time-domain oscillations achieved by the default and S3 configurations ($\phi(t = 0) = 0.1$ rad).

It is worth to check the physical behavior employing the two configurations in Table 2. An initial perturbation to the torsional-roll DOF ($\phi(t = 0) = 0.1$ rad) is used to excite the transient response of the gear. Fig. 6 illustrates the response in torsional-yaw deflection ψ, lateral bending

displacement y_a, torsional-roll deflection δ and tire lateral deflection v_1. It can be observed that while the frequency-based optimization suggests a significant improvement in the least damping ratio with S3, this does not result in an improved transient response due to a larger response to a lower-frequency mode. This suggests that the convenience of the frequency-domain analysis is limited for this problem, as the mode shapes are significantly altered when certain suppression devices are added.

IV. Time-domain optimization results

In this section, time-domain optimization results relating to the performance benefits of shimmy suppression devices incorporating inerters are presented. Two perturbations, which are applied to the tire and can trigger shimmy oscillations, are used to excite the transient response. There are a wide range of cost functions that could be used in the optimization. To demonstrate the potential of an inerter-based device we select the peak amplitude and settling time of the torsional-yaw response as the cost functions. However we recognize that for a full design study a more complex optimization with multiple performance criteria would be used.

A. Initial operation conditions and time-domain performance criteria

Two types of initial conditions are considered in this study. Firstly, we assume the tire travelling direction is disturbed suddenly, causing a corresponding initial input to the tire slip angle α. As presented in Section II, $\alpha = \alpha^{'}$ when the MLG is in undisturbed state. Hence, $\alpha(t=0) = \alpha^{'}(t=0) = 0.1\,\text{rad}$ is used as the first type of excitations to the system. This input will be referred to as the 'slip input'. The second input, the 'side force input', is an initial side force $F_y^{'} = 1.0 \times 10^7\,\text{N}$ applied in the Y direction to the wheel axle for 1 ms. Note that all the states, except for the excited one, are set to zero initially.

The torsional-yaw motion is oftenly regarded as of significant importance for the gear fatigue life [35]. Therefore, the time-domain optimization focuses on investigating the effectiveness of the proposed device on the torsional-yaw motion. The performance measures are defined as i) the peak magnitude and ii) the settling time of the torsional-yaw motion. As the transient response to a perturbation is considered, the maximum amplitude of the torsional-yaw response, ψ_{peak}, is an

important measure of the response. Also the time during which the vibration is above a certain threshold, the settling time t_{settle}, gives a measure of the duration of undesirable behavior following a perturbation. In this paper, t_{settle} is defined as the time duration spent when the amplitude of the response exceeds $\pm 10\%$ of ${\psi_{peak1,2}}^*$, where ${\psi_{peak1,2}}^*$ is the peak response amplitude for the system with the default shimmy damper under the initial tire slip angle input and side force input, respectively. It can be calculated that ${\psi_{peak1}}^* = {\psi_{peak2}}^* = 1.5$ rad. Note there are a number of ways in which such performance could be addressed such as setting an acceptable threshold amplitude of vibration. However such a criterion would be perturbation amplitude dependent, giving rise to the challenge of selecting a "reasonable" size of perturbation. Instead we adopt the more general, and amplitude independent, settling time criterion which can be regarded as a measure of effective damping in the linear system analysis. Each of these two measures, peak amplitude and settling time, will be used as a cost function with the constraint that the other measure must be no worse than the value achieved with the default shimmy damper.

B. Baseline improvement by geometric modifications

From the existing literature, the gear geometry plays an important role in stabilizing shimmy-prone gears (see [36] for example). In order to have a benchmark with which the improvement of inerter-based shimmy suppression device can be compared, two key MLG geometry parameters, wheel distance l and mechanical trail e, are varied. Default shimmy suppression device and its parameter values are used. The two geometry parameters are varied by $\pm 30\%$ from their nominal values.

The slip input is firstly considered. The time-histories of the torsional-yaw motion are plotted for the off-nominal wheel distance cases in Fig. 7. It is observed that the variation of corresponding transient responses is very limited even when large changes in l are applied. Decreasing the wheel distance results in marginally smaller magnitudes of torsional-yaw motion and the response decays more quickly. The biggest improvements on ψ_{peak} and t_{settle} obtained are 2.0% and 14.5%, respectively. Similar trends can be observed for the case that the mechanical trail is varied. With a 30% reduction of e leading to improvements in both performance measures – 11.3% for ψ_{peak} and 14.4%

for t_{settle}. This suggests that improvements obtained by modifying the shimmy suppression device in the order of 10% or more for either performance measure may be thought of as significant.

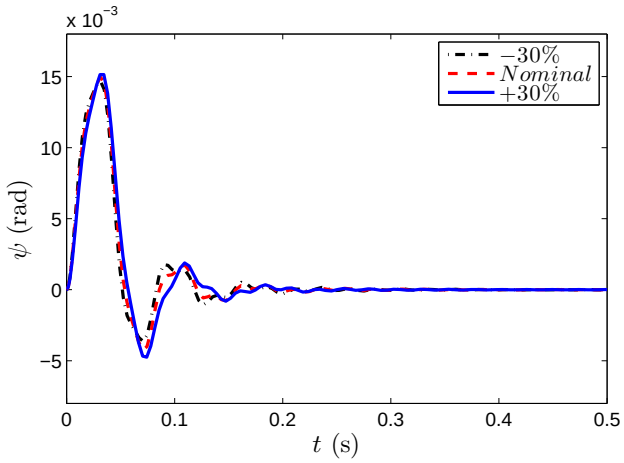

Fig. 7 Comparison of ψ time series varying l for the system with a default shimmy damper configuration.

C. Optimization results and beneficial shimmy suppression configurations

By using the optimization and simplification procedures discussed in Section II.C, layout S2 has been identified as with promising benefits. For clarity, the subscripts α and F are used to specify the optimization results obtained for the slip input and side force input, respectively. Also, the subscript p (s) is used to represent the optimization results using the peak amplitude (the settling time) as cost function.

1. Slip input

Rows 2 and 3 of Table 3 summarize the optimal results for improving ψ_{peak}. It can be seen that taking the traditional layout S1, and optimizing the spring and damper for this performance criteria results in a 16.7% reduction of ψ_{peak} over the default shimmy damper. With the layout S2, the improvement increases to 28.0%. This significant improvement can be observed from the time series responses illustrated in Fig. 8a.

However, note that the second peak magnitude of the yaw response is increased significantly compared with the default response, especially with the S2$_{\alpha p}$ configuration. Hence, an extra re-

striction is included where the second peak amplitude should be no bigger than that for the default shimmy damper. Here a subscript p^* is used to denote this new optimization. The p^* optimization cases are presented in rows 4 and 5 of Table 3 and the improved responses are illustrated in Fig. 8b. It can be seen that the second peak amplitude is noticeably smaller than that in Fig. 8a. As expected, the trade-off between ψ_{peak} and the second peak amplitude leads to slightly smaller improvement in ψ_{peak}. However, the improvement by the inerter-based scheme $S2_{\alpha p^*}$, 26.7% over the default system, is still significant. Note again that the peak amplitude optimization problem can be refined in different ways, while maintaining the emphasis on minimizing the peak amplitude. Here we choose to limit the second peak so that it is no larger than that for the default response, an alternative approach could be to look at the peak-to-peak amplitude, although this would not necessarily result in a maintained or reduced second peak.

Table 3 Optimization results and involved parameter values for the slip input case[§]

Layouts	Performance		Optimum parameter values		
	ψ_{peak}	t_{settle}	k	c	b
	$\times 10^{-2}$ rad	$\times 10^{-1}$ s	$\times 10^{5}$ N·m/rad	$\times 10^{3}$ N·m·s/rad	N·m·s^2/rad
Default	1.5	1.1	1.9	7.4	-
$S1_{\alpha p}$	1.25(16.7%)	1.08	1.1	14.4	-
$S2_{\alpha p}$	1.08(28.0%)	0.96	3.1	1.5	341
$S1_{\alpha p^*}$	1.3(13.3%)	1.01	1.4	11.8	-
$S2_{\alpha p^*}$	1.1(26.7%)	1.04	7.2	13.0	145
$S1_{\alpha s}$	1.5	0.93(15.5%)	1.1	8.2	-
$S2_{\alpha s}$	1.25	0.47(57.3%)	2.4	8.2	50

[§] % improvements are given in bracket for the criteria being optimized.

Rows 6 and 7 of Table 3 present the settling time improvements provided by $S1_{\alpha s}$ and $S2_{\alpha s}$. A considerable improvement in t_{settle}, 57.3%, is achieved with $S2_{\alpha s}$ scheme while $S1_{\alpha s}$ can only achieve 15.5% improvement. The time series for the torsional-yaw response are shown in Fig. 8c. Note that the response achieved with $S2_{\alpha s}$ decays more quickly and at the same time has a good ψ_{peak} performance. It can be noticed that $S2_{\alpha s}$ can lead to a 16.7% improvement of ψ_{peak}. Taking

this into consideration, it could be argued that $S2_{\alpha s}$ is more beneficial over other schemes in Table 3.

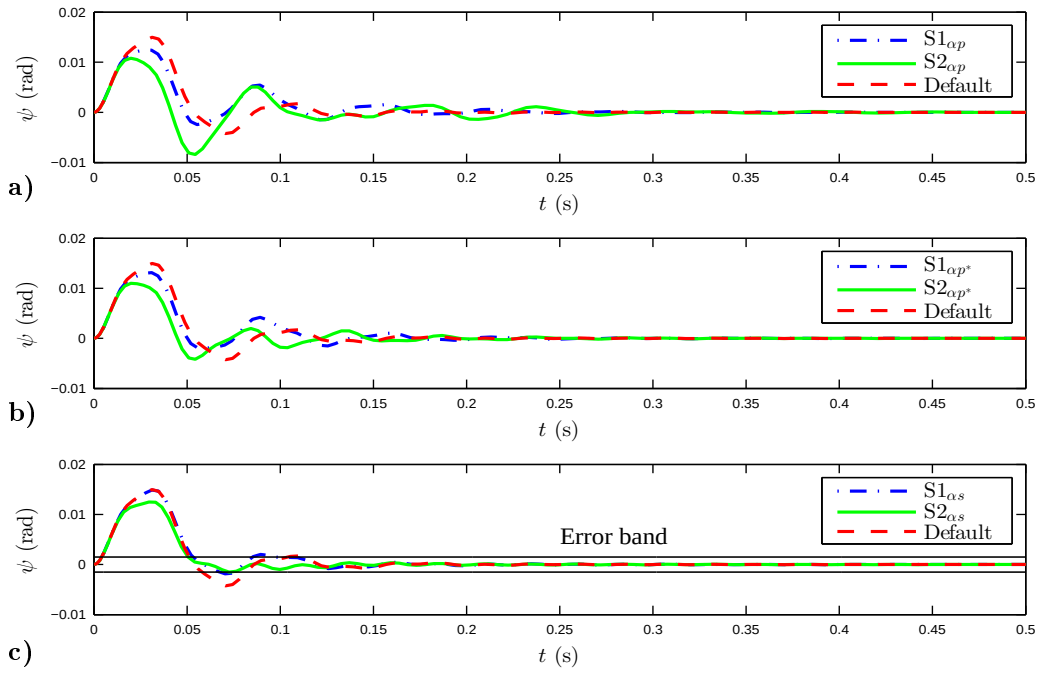

Fig. 8 Comparison of ψ time series for the default and beneficial schemes excited by the slip input.

2. Side force input

Similar to the slip input case, the optimization will be performed for the two cost functions separately when the system is excited by an impulsive side force. The optimization results when minimizing ψ_{peak} are summarized in rows 2 and 3 of Table 4. Arguably the configuration with a parallel inerter-spring-damper layout is beneficial when compared with the optimal S1 configuration, with a 32.0% improvement over the default device. The responses provided by two optimized schemes are shown in Fig. 9a. As before, an increased second peak is observed when optimizing the S2 layout. To address this, further optimization is performed in which the second peak of the response is restricted to be no greater than that for the default system. The results have been shown in rows 4 and 5 of Table 4 and the torsional-yaw response is shown in Fig. 9b. Here, by limiting the second peak of ψ response the improvement of ψ_{peak} is reduced, but still significant – 16.7% by $S2_{Fp^*}$.

Table 4 Optimization results and involved parameter values for the side force input case¶

Layouts	Performance		Optimum parameter values		
	$\times 10^{-2}$ rad	$\times 10^{-1}$ s	$\times 10^{5}$ N·m/rad	$\times 10^{3}$ N·m·s/rad	N·m·s^2/rad
Default	1.5	1.22	1.9	7.4	-
S1$_{Fp}$	1.4(6.7%)	1.22	3.5	8.6	-
S2$_{Fp}$	1.02(32.0%)	1.22	3.9	16.2	388
S1$_{Fp^*}$	1.4(6.7%)	1.22	2.5	9.4	-
S2$_{Fp^*}$	1.25(16.7%)	0.97	4.5	10.0	84
S1$_{Fs}$	1.4	1.22(0.2%)	1.2	10.3	-
S2$_{Fs}$	1.5	0.85(30.3%)	1.6	62.8	19

¶ % improvements are given in bracket for the criteria being optimized.

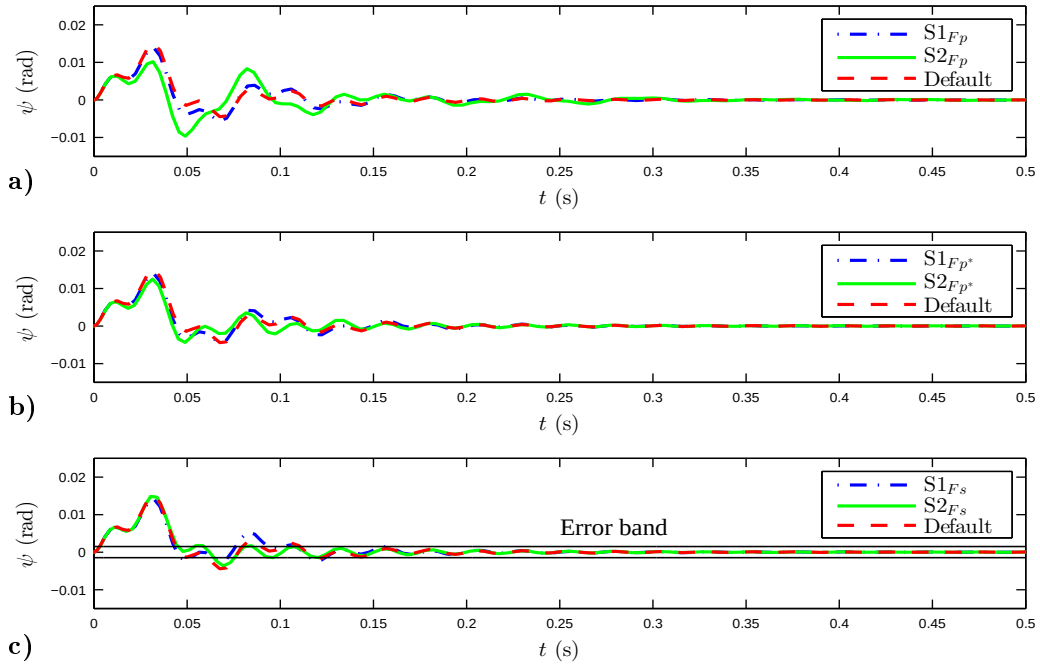

Fig. 9 Comparison of ψ time series for the default and beneficial schemes excited by the side force input

The improvements of t_{settle} achieved by S1$_{Fs}$ and S2$_{Fs}$ are summarized in rows 6 and 7 of Table 4, along with the optimized parameter values and the response illustrated in Fig. 9c. It can be seen that the t_{settle} achieved using the optimal S1 is close to that for the default system

with only 0.2% improvement. For the parallel inerter-spring-damper configuration, $S2_{Fs}$, a 30.3% improvement is obtained. On the other hand, it can be observed that $S2_{Fs}$ does not provide any improvement of ψ_{peak}, while both performance measures are improved with $S2_{Fp^*}$, 16.7% improvement on ψ_{peak} and 20.5% improvement on t_{settle}. Arguably, here the $S2_{Fp^*}$ is the most beneficial preferable suppression configuration in Table 4.

D. Overall beneficial configurations

Based on the results presented in Section IV.C, $S2_{\alpha s}$ and $S2_{Fp^*}$ are proposed as the beneficial configurations for the slip input and the side force input, respectively. It is still worth to check the performance with the slip input and side force input for $S2_{Fp^*}$ and $S2_{\alpha s}$, respectively. Table 5 summarizes the improvements of the two performance measures provided by $S2_{\alpha s}$ and $S2_{Fp^*}$ along with the two optimal spring-damper configurations, $S1_{\alpha s}$ and $S1_{Fp^*}$. The percentage improvements are compared with the default shimmy damper and both initial conditions are considered. The table shows that the inerter-based configurations provide larger benefits over the two optimal spring-damper configurations. Moreover, when applying the other input, both schemes still provide benefits using either performance measure. Figure 10 illustrates the comparison of ψ time series produced by the four beneficial schemes when the system is excited by the slip input and the side force input. From the time-domain response, it can be seen that with both kinds of inputs, $S2_{\alpha s}$ and $S2_{Fp^*}$ are always capable of providing performance advantages: experiencing smaller peak amplitudes and quicker settling.

Table 5 Improvement achieved by four optimal configurations under two initial inputs

Configurations	Slip input		Side force input	
	Impro. of ψ_{peak}, %	Impro. of t_{settle}, %	Impro. of ψ_{peak}, %	Impro. of t_{settle}, %
$S1_{\alpha s}$	0.7	14.9	0	0
$S2_{\alpha s}$	16.7	57.3	9.1	1.0
$S1_{Fp^*}$	8.7	0.36	6.7	0.08
$S2_{Fp^*}$	24.5	33.8	16.7	20.5

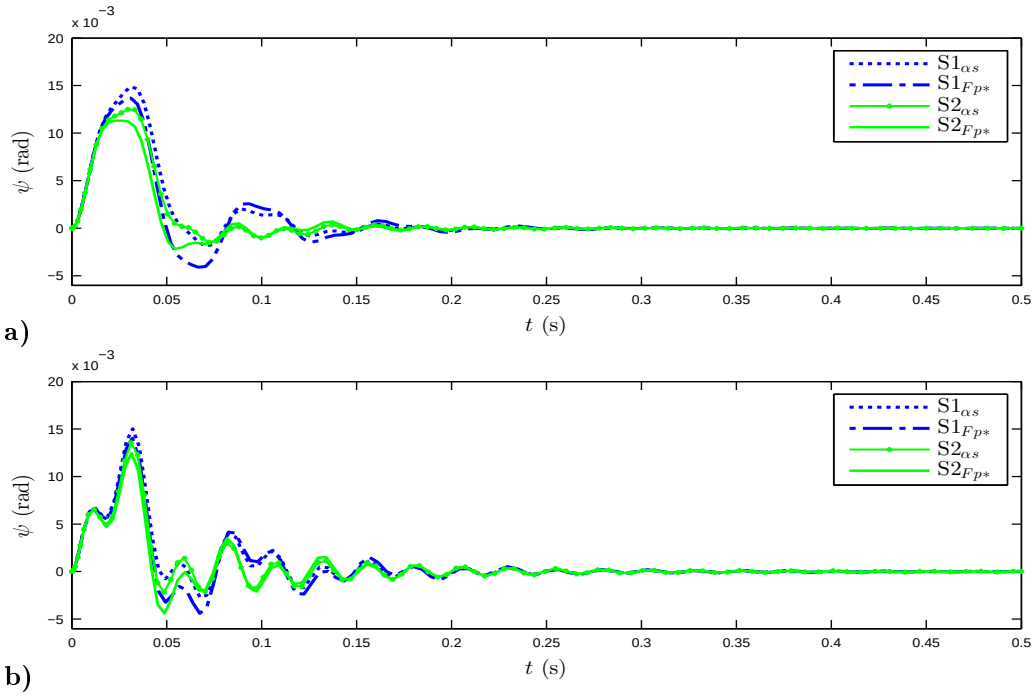

Fig. 10 Comparison of ψ time series excited by a) the slip input and b) the side force input.

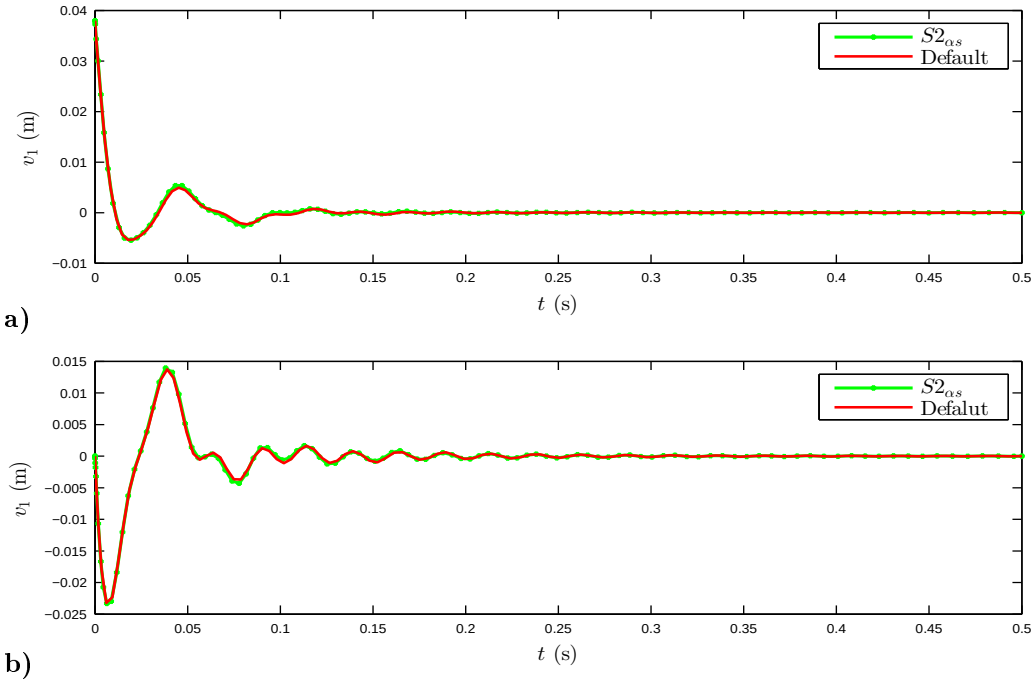

Fig. 11 Comparison of v_1 time series excited by a) the slip input and b) the side force input.

Since the tire motion plays an importance role on tire-ground contact dynamics, it is worth to check the effect of the proposed configuration on the tire lateral motion. Figure 11 illustrates the

comparison of the tire lateral response v_1 for the default and the beneficial configuration (using $S2_{\alpha s}$ as an example). It can be seen that the responses are almost the same compared with the default shimmy damper, which reflects the fact that the torsional-yaw motion is to a large extent decoupled from the tire lateral motion in this model. Hence, the modification of the shimmy suppression device has minimal impact on this motion.

V. Conclusions

The main focus of this study is the potential benefits of the shimmy suppression devices incorporating inerters. Apart from the shimmy suppression device motion, the MLG torsional-yaw, lateral, torsional-roll motions and the tire dynamics are all taken into consideration. Results of eigenvalue optimization are presented to demonstrate the limitation of frequency-domain analysis for this problem. Hence time-domain optimization is proposed. Using the maximum amplitude and the settling time of the torsional-yaw motion as cost functions, optimization procedure is carried out. When the slip input is applied, a 16.7% improvement on the peak amplitude and 57.3% improvement on the settling time are obtained using a parallel inerter-spring-damper configuration. If the system is excited by the side force input, the parallel inerter-spring-damper layout with optimized parameter values provides 16.7% improvement on the peak amplitude and 20.5% improvement on the settling time. These benefits exceed those obtained by making significant changes to the gear geometry. It needs to be emphasized that the two beneficial configurations also provide performance advantages when the other non-optimized input is applied. Based on the optimization results, it can also be seen that the identified inerter-based configurations are more beneficial than the optimized parallel spring-damper configurations. In general, the aim of this paper is to show the potential of an inerter-based device. This has been achieved using the two example optimization criteria. For a full optimization study as part of a landing gear design process, the criteria would need to be adjusted based on the performance requirements drawn up by the aircraft manufacture. In the future work, the nonlinearities, including the nonlinear tire model, could be considered since it may lead to more coupling between different modes. It would also be interesting to include the nonlinear damping into the suppression device due to its superior energy dissipation characteristics.

Acknowledgements

The authors would like to acknowledge the support of the EPSRC and the China Scholarship Council: Simon Neild is supported by an EPSRC fellowship EP/K005375/1 and Yuan Li is supported by a China Scholarship Council studentship.

References

[1] Woerner, P., and Noel, O., "Influence of Nonlinearity on the Shimmy Behaviour of Landing Gear," AGARD-R-800, 1996.

[2] Broulhiet, G., "The Suspension of the Automobile Steering Mechanism: Shimmy and Tramp," *Bulletin of Society of Civil Engineers*, Vol. 78, 1925, pp. 540–554 (in French).

[3] Moreland, W.J., "The Story of Shimmy," *Journal of the Aeronautical Sciences*, Vol. 21, No. 12, 1954, pp. 793–808. doi: 10.2514/8.3227

[4] Pacejka, H.B., "Analysis of the Shimmy Phenomenon," *Proceedings of the Institution of Mechanical Engineers: Automobile Division*, Vol. 180, No. 1, 1965, pp. 251–268.

[5] Smiley, R. F., "Correlation, Evaluation, and Extension of Linearized Theories for Tire Motion and Wheel Shimmy," NACA Rept. 1299, 1957.

[6] Von Schlippe, V. B., and Dietrich, R., "Shimmying of a Pneumatic Wheel," NACA TM-1365, 1954, pp. 125–160.

[7] Fromm, H., "Brief Report on the History of the Theory of Shimmy," NACA TM-1365, 1954, pp. 181–189.

[8] Besselink, I.J.M., "Shimmy of Aircraft Main Landing Gear," Ph.D. Dissertation, Delft Univ. of Technology, The Netherlands, 2000.

[9] Hitch, H.P.Y., "Aircraft Ground Dynamics," *Vehicle System Dynamics*, Vol. 10, No. 4–5, 1981, pp. 319–332. doi: 10.1080/00423118108968681

[10] Glaser, J., and Hrycko, G., "Landing Gear Shimmy–De Havilland's Experience," AGARD-R-800, 1996.

[11] Van Der Valk, R., and Pacejka, H. B., "An Analysis of a Civil Aircraft Main Gear Shimmy Failure," *Vehicle System Dynamics*, Vol. 22, No. 2, 1993, pp. 97–121. doi: 10.1080/00423119308969023

[12] Jocelyn, P., "Overview of Landing Gear Dynamics," *Journal of Aircraft*, Vol. 38, No. 1, 2001, pp.130–137. doi: 10.2514/2.2744

[13] Sura, N.K., and Suryanarayan, S., "Lateral Stability of Aircraft Nose-wheel Landing Gear with Closed-loop Shimmy Damper," *Journal of Aircraft*, Vol. 46, No. 2, 2009, pp.505–509. doi: 10.2514/1.37626

[14] Feng, F., Nie, H., Zhang, M., and Peng, Y., "Effect of Torsional Damping on Aircraft Nose Landing-Gear Shimmy," *Journal of Aircraft*, Vol. 52, No. 2, 2014, pp. 561–568. doi: 10.2514/1.C032772

[15] Padmanabhan, M.A., and Dowell, E.H., "Landing Gear Design/Maintenance Analysis for Nonlinear Shimmy," *Journal of Aircraft*, Vol. 52, No. 5, 2015, pp. 1707–1710. doi: 10.2514/1.C033027

[16] Houlston, P.R., Garvey, S.D., and Popov, A.A., "Modal Control of Vibration in Rotating Machines and Other Generally Damped Systems," *Journal of Sound and Vibration*, Vol. 302, No. 1, 2007, pp. 104–116. doi: 10.1016/j.jsv.2006.11.013

[17] Pouly, G., Huynh, T.H., Lauffenburger, J.P., and Basset, M., "Indirect Fuzzy Adaptive Control for Active Shimmy Damping," *17th IFAC World Congress*, Vol. 95, July, 2008. doi: 10.3182/20080706-5-KR-1001.02548

[18] Smith, M.C., "Synthesis of Mechanical Networks: the Inerter," *Automatic Control*, Vol. 47, No. 10, IEEE, 2002, pp. 1648–1662. doi: 10.1.1.227.7188

[19] Jiang, J.Z., Matamoros-Sanchez, A.Z., Goodall, R.M., and Smith, M.C., "Passive Suspensions Incorporating Inerters for Railway Vehicles," *Vehicle System Dynamics*, Vol. 50, No. sup1, 2012, pp. 263–276. doi: 10.1080/00423114.2012.665166

[20] Jiang, Z., Matamoros-Sanchez, A.Z., Zolotas, A., Goodall, R., and Smith, M.C., "Passive Suspensions for Ride Quality Improvement of Two-axle Railway Vehicles," *Proceedings of the Institution of Mechanical Engineers, Part F: Journal of Rail and Rapid Transit*, 2013. doi: 10.1177/0954409713511592

[21] Scheibe, F., and Smith, M.C., "Analytical Solutions for Optimal Ride Comfort and Tyre Grip for Passive Vehicle Suspensions," *Vehicle System Dynamics*, Vol. 47, No. 10, 2009, pp. 1229–1252. doi: 10.1080/00423110802588323

[22] Jiang, J.Z., Smith, M.C., and Houghton, N.E., "Experimental Testing and Modelling of a Mechanical Steering Compensator," *3rd IEEE International Symposium on Communications, Control and Signal Processing*, 2008, pp. 249–254. doi: 10.1.1.228.9199

[23] Limebeer, D., Sharp, R., Evangelou, S., and Smith, M., "An H-∞ Loop-Shaping Approach to Steering Control for High-Performance Motorcycles", *Lecture Notes in Control and Information Sciences*, Vol. 329, 2006, pp. 257–275.

[24] Lazar, I.F., Neild, S.A., and Wagg, D.J., "Using an Inerter-based Device for Structural Vibration Suppression," *Earthquake Engineering & Structural Dynamics*, Vol. 43, No. 8, 2014, pp. 1129–1147.

[25] Wang, F.C., Chen, C.W., Liao, M.K., and Hong, M.F., "Performance Analyses of Building Suspension Control with Inerters," *46th IEEE Conference on Decision and Control*, IEEE, 2007, pp. 3786–3791. doi: 10.1109/CDC.2007.4434186

[26] Mcbeath, S., "Shocks to the System," Racecar Engineering, Nov. 2011.

[27] Terkovics, N., Neild, S., Lowenberg, M., and Krauskopf, B., "Bifurcation Analysis of a Coupled

Nose-Landing-Gear-Fuselage System," *Journal of Aircraft*, Vol. 51, No. 1, 2014, pp.259–272. doi: 10.2514/1.C032324

[28] Currey, N.S., "Aircraft Landing Gear Design: Principles and Practices," AIAA Education Series, Washington, 1988.

[29] Bott, R., and Duffin, R.J., "Impedance Synthesis Without Use of Transformers," *Journal of Applied Physics*, Vol. 20, No. 8, 1949, pp. 816–816.

[30] Storer, J.E., "Passive Network Synthesis," McGraw-Hill, New York, 1957, pp. 298–302.

[31] Van Valkenburg, M.E., "Introduction to Modern Network Synthesis," Wiley, New York, 1960.

[32] Jiang, J.Z., and Smith, M.C., "Regular Positive-real Functions and Five-element Network Synthesis for Electrical and Mechanical Networks," *Automatic Control*, Vol. 56, No. 6, IEEE, 2011, pp. 1275–1290. doi: DOI: 10.1109/TAC.2010.2077810

[33] Jiang, J.Z., and Smith, M.C., "Series-parallel Six-element Synthesis of Biquadratic Impedances," *Circuits and Systems I: Regular Papers*, Vol. 59, No. 11, IEEE, 2012, pp. 2543–2554. doi: 10.1109/TCT.1971.1083257

[34] Zhang, S.Y., Jiang, J.Z., and Neild, S.A., "Optimal Configurations for a Linear Vibration Suppression Device in a Multi-storey Building," *Structural Control and Health Monitoring*, 2016.

[35] "Landing Gear Stability," Society of Automotive Engineers, Gears, Struts And Couplings Committee A-5B, Aerospace Landing Gear Systems, Rept. SAE AIR 4894.

[36] Roe, G.E., and Thorpe, T.E., "Experimental Investigation of the Parameters Affecting the Castor Stability of Road Wheels," *Journal of Mechanical Engineering Science*, Vol. 15, No. 5, 1973, pp. 365–369.